

Al-Mg-Zn 钎料钎焊镁合金 AZ31B 接头的显微组织和性能

马 力¹, 贺定勇¹, 李晓延¹, 蒋建敏¹, 王立志²

(1. 北京工业大学 材料科学与工程学院, 北京 100124;
2. 中冶集团建筑研究总院 焊接所, 北京 100088)

摘 要: 以 Al-Mg-Zn 钎料对变形镁合金 AZ31B 进行了高频感应钎焊, 分析了变形镁合金 AZ31B 钎焊接头的显微组织、钎缝物相和力学性能。采用扫描电镜(SEM)、X 射线衍射仪(XRD)、X 射线能谱分析仪(EDS)等仪器分析了钎焊接头的界面组织及钎缝生成相, 测试了接头的强度及形成相的显微硬度。结果表明, 在钎焊接头的钎缝中钎料与母材 AZ31B 发生反应生成离异共晶组织 $\alpha\text{-Mg}+\beta\text{-Mg}_{17}(\text{Al}, \text{Zn})_{12}$, 母材 AZ31B 的显微硬度最低, 钎缝中的 $\beta\text{-Mg}_{17}(\text{Al}, \text{Zn})_{12}$ 相显微硬度最高。对接和搭接接头断口的断裂形式为沿晶脆性断裂, 断裂产生在离异共晶组织 $\alpha\text{-Mg}+\beta\text{-Mg}_{17}(\text{Al}, \text{Zn})_{12}$ 中的 $\beta\text{-Mg}_{17}(\text{Al}, \text{Zn})_{12}$ 硬脆相处。

关键词: AZ31B 镁合金; Al-Mg-Zn 钎料; 钎焊; 离异共晶; 接头强度

中图分类号: TG454 文献标识码: A 文章编号: 0253-360X(2009)11-0061-04



马 力

0 序 言

镁及其镁合金的钎焊方法主要有火焰钎焊、炉中钎焊、浸沾钎焊等。与其它金属相比镁合金的钎焊较困难, 其原因在于镁对氧的亲合力极大, 成为镁合金钎焊时的主要难点之一^[1-3]。通常, 镁合金的钎焊在接头强度要求不高的场合采用软钎焊, 对接头强度要求比较高时则采用硬钎焊。美国焊接学会列举的目前可用于镁合金钎焊的商业钎料有 BMg-1 和 BMg-2a。但这两种钎料的熔点都比较高, 钎焊温度在 600℃左右, 与这两种钎料共同使用的钎剂熔点温度也较高(约 538℃), 超过大多数镁合金的燃点及熔点温度, 因此它们只适于钎焊几种镁合金, 并不适于钎焊熔点低的镁合金。日本研发了用于钎焊 AZ31B 镁合金的低熔点钎料^[4,5], 钎料熔点小于 480℃, 但该钎料中铟用量太大, 价格昂贵, 且不易获得。所以熔点较低并且价格低廉的镁合金钎料的开发就成为了一个重要的研究方向。作者采用自行研制的一种 Al-Mg-Zn 钎料对镁合金 AZ31B 进行了高频感应钎焊。分析了钎焊接头的显微组织和力学性能, 分析了钎焊接头断裂的原因。

1 试验方法

试验在氩气保护的条件下进行高频感应钎焊, 采用 SP-35AB 高频感应加热装置, 氩气流量为 0.3 L/min。母材采用热轧 AZ31B 变形镁合金板材, 板厚 3.3 mm, AZ31B 的固相点温度为 566℃, 液相点温度为 627℃, AZ31B 变形镁合金的化学成分如表 1 所示。钎焊接头试样尺寸按国家标准 GB11363-89 执行, 试样尺寸大小为 80 mm×24 mm×3.3 mm。试验钎料熔炼在 SG2-7.5-12 型坩埚电阻炉中进行。熔炼完成后, 在金属型中浇注成形。钎料化学成分为 Al56.6, Mg29.7, Zn13.7(质量分数, %)。用 WCR-DTA 差热分析仪测得钎料固相点温度为 448℃, 液相点温度为 463℃。

表 1 AZ31B 镁合金化学成分(质量分数, %)
Table 1 Chemical composition of AZ31B magnesium alloy

Al	Zn	Mn	Si	Ni	Fe	Mg
2.50~3.50	0.50~1.50	0.20~0.50	0.10	0.01	0.01	余量

QJ201 作为钎焊的钎剂, QJ201 的化学成分为 50%KCl, 32%LiCl, 10%NaF, 8%ZnCl₂(质量分数)。QJ201 的熔点范围为 460~620℃。试验钎焊温度为

480 ~ 550 ℃, 试验钎焊时间为 150 s, 高频感应钎焊后在感应加热装置内的钎焊接头试样持续通氩气保护冷却至室温, 取出焊好的钎焊接头试样用清水冲洗掉残留的钎剂. 采用 HXD — 1000 显微硬度计测试钎焊接头界面的显微硬度. 用 MAGIX — PW2403 型 X 荧光光谱分析仪分析钎缝的化学成分. 采用 JEOLJSM6500F 型扫描电镜 (配 EDS) 和 D8ADVANCE 型旋转阳极 X 射线衍射分析仪对钎焊接头的显微组织、钎缝物相组成进行分析, 钎焊接头的力学性能测试采用 MTS — 810 材料测试系统.

2 试验结果与分析

2.1 钎焊接头组织分析

钎焊搭接接头的界面组织形貌如图 1 所示, 扩散区和母材 AZ31B 之间形成了不是很明显的界限. 界面区中的金属间化合物向母材侧呈枝状生长. 界面钎缝中心区有不连续网状分布的粗大金属间化合物生成, 这些金属间化合物主要分布在基体的晶界处.

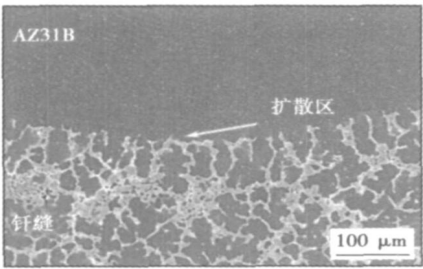


图 1 钎焊界面显微组织形貌
Fig 1 Interface microstructure of brazing

钎焊接头的元素线扫描图像 (图 2 中白线 AB 位置) 如图 2 所示. 从图 2 中可以看出, 在钎缝侧基体内 Mg 元素含量要高于金属间化合物处的 Mg 元素含量, 钎缝侧金属间化合物处 Mg 元素的含量最低, 钎缝侧 Mg 元素含量和母材侧的 Mg 元素含量相当, 母材侧的 Mg 元素含量略高, 说明母材侧的 Mg 元素在钎焊过程中已经向钎缝侧的液态钎料大量溶解. 钎缝侧 Al 元素含量比母材侧的 Al 元素含量高, 钎缝侧 Al 元素主要分布在金属间化合物上. 推测一部分 Al 元素与 Mg、Zn 元素形成金属间化合物相, 另一部分则固溶在基体中. 钎缝侧 Zn 元素也是主要分布在金属间化合物上. 推测一部分 Zn 元素与 Mg、Al 元素形成金属间化合物相, 另一部分则固溶在基体中.

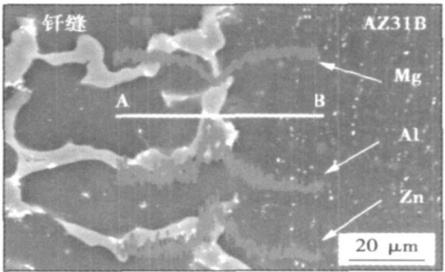


图 2 钎焊界面线扫描图像
Fig 2 Element line scanning images of interface

2.2 钎焊接头钎缝物相分析

钎焊后测得钎缝的化学成分为 Mg78.0, Al18.0, Zn4.0 (质量分数, %). 和原始钎料化学成分 Al56.6, Mg29.7, Zn13.7 (质量分数, %) 相比, 钎缝的化学成分中 Mg 元素含量大量增加. 说明钎料在钎焊被加热熔化过程中, 母材侧的 Mg 元素大量溶解进钎料形成钎缝组织时, 致使钎焊接头钎缝中的 Mg 元素含量上升, Mg 元素含量上升的同时对钎缝中的 Al、Zn 元素产生了稀释作用, 从而导致 Al、Zn 元素相对含量下降. 钎焊接头的 XRD 分析结果如图 3 所示, 钎缝的组成相为 α -Mg 相和 β -Mg₁₇(Al, Zn)₁₂ 相. 由 Mg-Al 二元合金相图可知^[6], 当温度低于液相线温度时, 合金开始凝固, 首先发生的是匀晶反应 $L \leftrightarrow \alpha$ -Mg, 初生的 α -Mg 相优先析出并长大, 先析出的 α -Mg 相溶解的 Al 原子含量低, 随着凝固的继续进行, 由于 Al 原子在固相中的扩散缓慢, 析出的 α -Mg 相的平均成分将偏离平衡固相线, 多余的 Al 原子被推向液体中. 随着温度的降低, 合金熔液在 437 ℃时将发生由液相转变为 α -Mg 相和 β -Mg₁₇Al₁₂ 相的共晶反应 $L \leftrightarrow \alpha$ -Mg + β -Mg₁₇Al₁₂. 在 437 ℃时 Al 原子在 Mg 原子中的溶解度最大, 达到 12.7%, 共晶点成分含 32.3% 的 Al 原子. 当温度低于 437 ℃

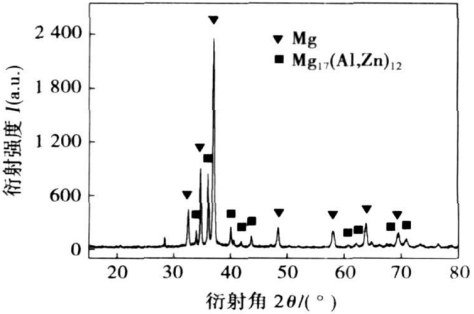


图 3 钎缝 XRD 图谱
Fig 3 XRD patterns of brazing seam

的固相线时,凝固并没有结束. 在共晶转变过程中 α -Mg 相将依附于先析出的 α -Mg 相生长,使共晶体组织中的 β -Mg₁₇Al₁₂ 相在 α -Mg 晶粒边界处独立长大,从而形成离异共晶组织. 随着温度的下降 Al 原子在 Mg 原子中的溶解度降低,100 °C 时降为 2.6%.

钎缝的显微组织形貌如图 4 所示,图 4 中 C 处区域基体 EDS 分析为 Mg95.75, Al3.38, Zn0.87(摩尔分数, %). C 处即为 α -Mg 相, α -Mg 相中固溶有 Al 元素和 Zn 元素. 图 4 中 D 处区域金属间化合物相 EDS 分析为 Mg59.62, Al35.45, Zn4.93(摩尔分数, %),其中 Mg:Al 的摩尔分数比和 β -Mg₁₇Al₁₂ 相中 Mg:Al 的摩尔分数比相比偏高. 而 D 处 Mg:(Al+Zn)的摩尔分数比更接近于 β -Mg₁₇Al₁₂ 相中 Mg:Al 的摩尔分数比 17:12. 此时 β -Mg₁₇Al₁₂ 相的化学表达式可表示为 β -Mg₁₇(Al, Zn)₁₂, 实际上 β -Mg₁₇(Al, Zn)₁₂ 是 β -Mg₁₇Al₁₂ 的扩展相^[7-9], 由于 Al, Zn 两元素的原子半径比较接近, β -Mg₁₇(Al, Zn)₁₂ 相是 β -Mg₁₇Al₁₂ 在冷却凝固过程中一部分 Al 原子被 Zn 原子取代后形成的. 图 4 中 EDS 分析也和图 2 中钎焊界面在金属间化合物处的 Mg, Al, Zn 三种元素线扫描图像的变化相吻合. β -Mg₁₇(Al, Zn)₁₂ 相和 β -Mg₁₇Al₁₂ 相具有相同的体心立方结构,两者点阵参数均为 1.054 nm. 故钎缝的离异共晶组织为 α -Mg + β -Mg₁₇(Al, Zn)₁₂, 钎缝的组成相为 α -Mg 相和 β -Mg₁₇(Al, Zn)₁₂ 相. 测得 AZ31B 母材侧的显微硬度平均值为 70 HV, 界面平均值为 124 HV, β -Mg₁₇(Al, Zn)₁₂ 相平均值为 183 HV, 钎缝侧 α -Mg 基体上平均值为 127 HV, 可见钎缝侧 α -Mg 基体和钎焊界面硬度相当, 母材侧 α -Mg 相显微硬度最低, 以沿 α -Mg 晶界网状形式存在的粗大 β -Mg₁₇(Al, Zn)₁₂ 相显微硬度最高.

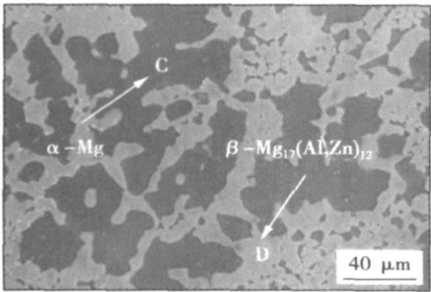


图 4 钎缝显微组织形貌

Fig 4 SEM microstructure of brazing seam

2.3 钎焊接头力学性能分析

实测对接接头平均抗拉强度为 45 MPa, 搭接接头平均抗剪强度为 27 MPa. 钎焊对接接头纵剖面断

口形貌如图 5 所示. 从图 5 中可以看出, 对接接头的断裂位置主要产生在沿 α -Mg 晶界网状分布的粗大 β -Mg₁₇(Al, Zn)₁₂ 相处. 对钎焊搭接接头纵剖面断口形貌分析后发现, 断裂位置也是主要产生在沿 α -Mg 晶界网状分布的粗大 β -Mg₁₇(Al, Zn)₁₂ 相处.

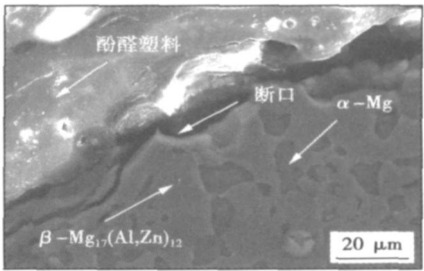


图 5 对接接头纵剖面断口形貌

Fig 5 SEM fractography of longitudinal profile of butted joint

钎焊对接接头拉伸断口形貌如图 6 所示. 图 6 中断口 E 处区域 EDS 分析为 Mg63.08, Al32.27, Zn4.65(摩尔分数, %). E 处 Mg:(Al+Zn)的摩尔分数比接近于 β -Mg₁₇Al₁₂ 相中 Mg:Al 的摩尔分数比 17:12. 即断口 E 处为 β -Mg₁₇(Al, Zn)₁₂ 相. 也可进一步证明断裂位置是产生在 β -Mg₁₇(Al, Zn)₁₂ 相处. 从图 6 中可以看出断口呈现出许多短而弯曲的撕裂棱, 撕裂棱两边由大小不一的解理台阶构成, 在断口上有二次裂纹, 这与钎焊接头组织的不均匀性有很大关系. 由于粗大的 β -Mg₁₇(Al, Zn)₁₂ 相以网状形式分布于 α -Mg 晶界, 而钎缝处的 β -Mg₁₇(Al, Zn)₁₂ 相是 β -Mg₁₇Al₁₂ 的扩展相, 只是 β -Mg₁₇Al₁₂ 相中的一部分 Al 原子被 Zn 原子取代. β -Mg₁₇Al₁₂ 相是硬脆相, β -Mg₁₇(Al, Zn)₁₂ 相和 β -Mg₁₇Al₁₂ 相性质相似, 也是硬脆相. 当钎焊接头受外力产生变形时, β -Mg₁₇(Al, Zn)₁₂ 相的协调变形能力很低, 难以与 α -Mg 基体协调一致地

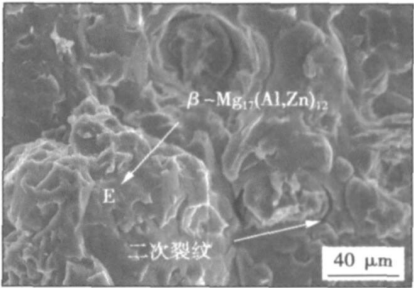


图 6 对接接头断口形貌

Fig. 6 SEM fractography of butted joint

变形,β-Mg₁₇(Al,Zn)₁₂相的脆性导致裂纹很容易形成与扩展,同时β-Mg₁₇(Al,Zn)₁₂相与α-Mg基体在界面处由于受到外力作用时易产生应力集中,在应力集中的作用下,使得硬脆β-Mg₁₇(Al,Zn)₁₂相沿α-Mg界面被拉开而产生裂纹,从而导致接头拉伸断口表现为较明显的沿晶脆性断裂特性.

3 结 论

(1) 以 Al-Mg-Zn 钎料在氩气保护条件下可以实现对变形镁合金 AZ31B 的高频感应钎焊.

(2) 钎缝中钎料与母材发生溶解与扩散反应生成离异共晶组织 α-Mg+β-Mg₁₇(Al,Zn)₁₂, 主要生成相为 α-Mg 相和 β-Mg₁₇(Al,Zn)₁₂相. 钎焊对接接头平均抗拉强度为 45 MPa, 搭接接头平均抗剪强度为 27 MPa.

(3) 钎焊对接和搭接接头的拉伸断口均表现为较明显的沿晶脆性断裂特性, 断裂主要产生在沿 α-Mg 晶界网状分布的粗大 β-Mg₁₇(Al,Zn)₁₂硬脆相处.

参考文献:

[1] Shapiro A E. Brazing magnesium alloys and magnesium matrix compos-
[6] Xu Q G, Wu B L, Zhang H F, *et al.* Wettability of molten Zr₃₅Cu₃₀Al₁₀Ni₅ on alumina and zirconia[J]. Rare Metals 2007, 26(3): 213—217.
[7] Shen P, Zheng X H, Lin Q L, *et al.* Wetting of polycrystalline α-Al₂O₃ by molten Zr₃₅Cu₃₀Al₁₀Ni₅ metallic glass alloy [J]. Metallurgical and Materials Transactions A, 2009, 40A: 444—449.
[8] Chase M W, Davies C A, Downey J R, *et al.* JANAF thermochemical tables [J]. Journal of Physical Chemistry Reference Data, 1985, 14(1): 156, 1691.

ites[J]. Welding Journal, 2005, 84(10): 33—43.
[2] Committee on brazing and soldering. Brazing manual[M]. Miami: American Welding Society, 1975.
[3] Cand I, Ame S M. Entwicklung von magnesium basis legierungen zum löten von leichtmetallen[D]. Aachen: Rheinisch Westfälische Technische Hochschule Aachen, 2005.
[4] Watanabe T, Komatu S, Yanagisawa A, *et al.* Development of flux and filler metal for brazing magnesium alloy AZ31B[J]. Yosetsu Gak-kai Ronbunshu/Quarterly Journal of the Japan Welding Society, 2004, 22(1): 163—167.
[5] Watanabe T, Komatu S, Oohara K. Development of flux and filler metal for brazing magnesium alloy AZ31B[J]. Welding Journal, 2005, 84(3): 37—40.
[6] Baker H. Alloy phase diagrams[M]. Ohio: Materials Park, 2006.
[7] Li Y, Terence G, Langdon. Creep behavior of an AZ91 magnesium alloy reinforced with alumina fibers [J]. Metallurgical and Materials Transactions A, 1999, 30(8): 2059—2066.
[8] Liu L M, Zhang Z D, Song G. Mechanism and microstructure of oxide fluxes for gas tungsten arc welding of magnesium alloy[J]. Metallurgical and Materials Transactions A, 2007, 38(3): 649—658.
[9] Czerwinski F, Zielinska L A, Pinet P J, *et al.* Correlating the micro-structure and tensile properties of a thixomolded AZ91D magnesium[J]. Acta Materialia, 2001, 49(7): 1225—1235.

作者简介: 马 力,男,1971 年出生,博士研究生. 主要从事镁合金钎焊材料及钎焊工艺研究. 发表论文 2 篇.

Email: mali2050@emails.bjtu.edu.cn

[上接第 60 页]

[6] Xu Q G, Wu B L, Zhang H F, *et al.* Wettability of molten Zr₃₅Cu₃₀Al₁₀Ni₅ on alumina and zirconia[J]. Rare Metals 2007, 26(3): 213—217.
[7] Shen P, Zheng X H, Lin Q L, *et al.* Wetting of polycrystalline α-Al₂O₃ by molten Zr₃₅Cu₃₀Al₁₀Ni₅ metallic glass alloy [J]. Metallurgical and Materials Transactions A, 2009, 40A: 444—449.
[8] Chase M W, Davies C A, Downey J R, *et al.* JANAF thermochemical tables [J]. Journal of Physical Chemistry Reference Data, 1985, 14(1): 156, 1691.

[9] Xian A P. Precursor film of tin-based active solder wetting on ceramics [J]. Journal of Materials Science, 1993, 28(4): 1019—1030.
[10] Durov A V, Naidich Y V, Kostyuk B D. Investigation of interaction of metal melts and zirconia [J]. Journal of Materials Science, 2005, 40(9—10): 2173—2178.

作者简介: 郑小红,女,1976 年出生,博士研究生. 主要研究方向为材料界面形成与控制. 发表论文 12 篇.

Email: xzheng1976@126.com

shaped and the thickness of IMC is much thinner when SAC0307 solder added 0.05% Ni is used. The consumption of Ni layer is nearly the same using both solders after the first time reflow soldering, but the residual thickness of the Ni layer in SAC0307/Ni solder is thinner than that in SAC0307-0.05Ni/Ni after aging for 384 h. So solders with a little Ni element can decrease the consumption rate of Ni layer effectively during aging, that is, the aging-resistant ability of Ni pad is improved obviously.

Key words: SAC0307-xNi; solder; Ni substrate; IMC; aging

Wettability of molten $Zr_{55}Al_{10}Ni_5Cu_{30}$ metallic glass brazing alloy on $\alpha-Al_2O_3$ and ZrO_2 ZHENG Xiaohong, SHEN Ping (Key Laboratory of Automobile Materials Ministry of Education, Jilin University, Changchun 130025, China). p 57—60, 64

Abstract: The wettability and interfacial characteristics of molten $Zr_{55}Al_{10}Ni_5Cu_{30}$ metallic glass brazing alloy on polycrystalline $\alpha-Al_2O_3$ and ZrO_2 substrates were studied using a modified sessile drop method. The results show that the wettability of the $Zr_{55}Al_{10}Ni_5Cu_{30}/\alpha-Al_2O_3$ system is excellent with the final contact angles approaching zero degree at 1 133-1 193 K. However, the wettability of the $Zr_{55}Al_{10}Ni_5Cu_{30}/ZrO_2$ system is poor, but it can be progressively improved with the elapse of time during the isothermal dwelling in the temperature range of 1 133-1 253 K. A certain extent of interfacial reaction happens in both systems. The investigation on the spreading kinetics and interfacial microstructure indicates that the adsorption of the active atoms such as Zr at the interface, particularly at the triple junctions, plays a key role in determining the wettability, whereas the contribution of the interfacial reaction is relatively minor.

Key words: Metallic glass brazing alloy; wettability; interfacial reaction; adsorption

Microstructure and mechanical properties of magnesium alloy AZ31B joint brazed with Al-Mg-Zn filler metal MA Li¹, HE Dingyong¹, LI Xiaoyan¹, JIANG Jianmin¹, WANG Lizhi² (1. College of Materials Science and Engineering, Beijing University of Technology, Beijing 100124, China; 2. Welding Research Institute of Central Research Institute of Building & Construction, China Metallurgical Group Corporation, Beijing 100088, China). p 61—64

Abstract: High-frequency induction brazing of wrought magnesium alloy AZ31B with Al-Mg-Zn filler metal was investigated. Microscopic structure, the phases and the mechanical properties of brazed joint were studied. The microstructure and formation phases at the interface in the brazed joint were investigated by scanning electron microscopy (SEM), X-ray diffraction instrument (XRD) and energy dispersive spectrometer (EDS). The strength of the brazed joint and the microhardness of the formation phases were also tested. The results show that Al-Mg-Zn filler metal reacting with the base metal AZ31B and $\alpha-Mg+\beta-Mg_{17}(Al, Zn)_{12}$ divorced eutectic structure is formed in the brazed joint. Microhardness of the base metal AZ31B is the smallest and $\beta-Mg_{17}(Al, Zn)_{12}$ phase of the brazed joint is the hardest. Both the butt joint and the overlap joint exhibit intergranular fracture mode, the fracture comes from hard brittle phase $\beta-Mg_{17}(Al, Zn)_{12}$ of $\alpha-Mg+\beta-Mg_{17}(Al, Zn)_{12}$ divorced eutectic structure.

Key words: AZ31B magnesium alloy; Al-Mg-Zn filler metal; brazing; divorced eutectic; joint strength

Failure of soldered joint during thermal fatigue test LIN Jian¹, LEI Yongping¹, ZHAO Haiyan², WU Zhongwei¹ (1. College of Materials Science and Engineering, Beijing University of Technology, Beijing 100124, China; 2. Department of Mechanical Engineering, Tsinghua University, Beijing 100084, China). p 65—68, 72

Abstract: The failure process of soldered joint in SMT was investigated by electrical resistance measurement method and crack observation method. The characteristics of electrical resistance value variation of lead-tin and lead-free soldered (SAC305) joints during the thermal fatigue test were obtained. And at the same time the crack propagation in soldered joint was observed. According to these measurements, the failure rules of lead-tin and lead-free soldered joint were compared. The relationship between electrical resistance value variation and crack propagation of soldered joint during thermal fatigue test was studied by FEM, and an empirical criterion to estimate the failure of the soldered joint in the thermal fatigue test was obtained based on electrical resistance value variation. The experimental results show that the lead-free soldered joint has a higher resistibility in thermal fatigue than the traditional lead-tin soldered joint. The criterion based on electrical resistance value variation was founded from the experimental and simulation results.

Key words: SMT; soldered joint; thermal fatigue; electrical resistance; crack

TiN/Ti composite coating deposited on titanium alloy substrate by reactive electric-spark HAO Jianjun^{1,2}, PENG Haibin¹, HUANG Jihua³, MA Yuejin¹, LI Jianchang¹ (1. College of Electromechanical Engineering, Agriculture University of Hebei, Baoding 071001, Hebei, China; 2. Light Metal Materials Engineering Research Center of Hebei, Baoding 071000, Hebei, China; 3. School of Materials Science and Engineering, University of Science and Technology of Beijing, Beijing 100083, China). p 69—72

Abstract: TiN/Ti composite coating was deposited on TC4 titanium alloy substrate with the self-made special gas-filled-closed electric-spark deposition device and electric-spark deposition machine modeled DZ-1400, the industry pure titanium (TA2) was used as electrode and the industry pure nitrogen gas as shielding and reacting atmosphere. The microstructures, interfacial behavior, phase and element in the coatings were investigated by scanning electronic microscope, X-ray diffraction and X-ray photo spectrum. The microhardness of coatings was tested and its wear-resistance property was tested by the self-made abrasion machine and compared with W18Cr4V rapid steel treated by quenching. The results show that an excellent bonding between the coating and substrate is ensured by the strong metallurgical interface. The coatings are mainly composed of Ti and synthesized TiN. The highest microhardness of coating reaches to 1 388 HV0.1, which is six times higher than that of the substrates. Wear resistance of the coatings is excellent.

Key words: reactive electric-spark deposition; TiN; composite coating; titanium alloy

Influence of transverse alternative magnetic field frequency on microstructure and properties of plasma arc surfacing layer

LIU Zhengjun, ZHAO Qian, CI Honggang, SU Yunhai (School of